LETTERS
PUBLISHED ONLINE: 22 MAY 2011 | DOI: 10.1038/NNANO.2011.78
nature nanotechnology

Discovery of superconductivity in $KTaO_3$ by electrostatic carrier doping

K. Ueno[1,2], S. Nakamura[3,4], H. Shimotani[5], H. T. Yuan[5], N. Kimura[4,6], T. Nojima[3,4], H. Aoki[4,6], Y. Iwasa[5,7] and M. Kawasaki[1,5,7]*

Superconductivity at interfaces has been investigated since the first demonstration of electric-field-tunable superconductivity in ultrathin films in 1960[1]. So far, research on interface superconductivity has focused on materials that are known to be superconductors in bulk[1–9]. Here, we show that electrostatic carrier doping can induce superconductivity in $KTaO_3$, a material in which superconductivity has not been observed before[10,11]. Taking advantage of the large capacitance of the self-organized electric double layer that forms at the interface between an ionic liquid and $KTaO_3$ (ref. 12), we achieve a charge carrier density that is an order of magnitude larger than the density that can be achieved with conventional chemical doping. Superconductivity emerges in $KTaO_3$ at 50 mK for two-dimensional carrier densities in the range 2.3×10^{14} to 3.7×10^{14} cm^{-2}. The present result clearly shows that electrostatic carrier doping can lead to new states of matter at nanoscale interfaces.

Chemical doping is the process of introducing electrical conductivity in an insulator by replacing atoms of one of the constituent elements with atoms of another element with a different valence state. To convert a Mott insulator, such as a cuprate, into a superconductor[13], it is necessary to achieve a dopant concentration of ~10% or 1×10^{21} dopant atoms per cm^3, but in many cases the chemical solubility of the insulator is too low to reach such concentrations. In addition, the replacement of some atoms during doping inevitably changes the crystalline structure and often introduces randomness into the system. Another way of donating charge carriers to an insulator is electrostatic doping by a field effect, as used in field-effect transistors (FETs). One can also accumulate mobile carriers at the surface of an insulator by applying a gate voltage V_G, but the gate dielectric breaks down when the electric field reaches a value of 1–10 MV cm^{-1}, which corresponds to a two-dimensional carrier density n_{2D} of $\sim 1 \times 10^{13}$ cm^{-2} (refs 3, 5, 14–16).

Recently, very high electric fields have been applied with an electric double-layer transistor, a device that uses a liquid electrolyte as a gate dielectric[17–19]. When a solid sample is immersed in this liquid electrolyte, a Helmholtz electric double layer (EDL) self-organizes at the interface (Fig. 1). This double layer can be thought of as a capacitor composed of a sheet of ions in the electrolyte and another sheet of accumulated image charges on the surface of the solid. These two layers are separated by less than 1 nm, which allows the EDL transistor to achieve values of n_{2D} as high as 8×10^{14} cm^{-2} within an electrostatic mechanism[12].

Figure 2a summarizes the relationship between the critical transition temperature T_c and three-dimensional carrier density n_{3D} for bulk superconductors that were converted from insulators by means of chemical or electrostatic doping. It is clear that the values of n_{3D} achieved by electrostatic doping are well above those needed to reach a superconducting state in the cuprates, so the EDL transistor should be able to induce superconductivity in insulators that cannot be made superconducting by chemical doping.

$KTaO_3$ is a promising candidate for superconductivity induced by electrostatic doping because it is similar to the low-n_{3D} superconductor $SrTiO_3$ in many ways: both have a perovskite structure, both have similar band structures, and both exhibit quantum paraelectricity[10,20]. It has also been shown that metallic conductivity can be induced in $KTaO_3$ at temperatures of ~10 K in conventional FET structures[21,22], but searches to temperatures as low as 10 mK have failed to find evidence for superconductivity in $KTaO_3$ (ref. 11). Insufficient carrier density is likely to be the reason why superconductivity has not yet been observed in $KTaO_3$: the tantalum ions in oxides have only one stable oxidation state (5+), in contrast to the three stable states (2+ , 3+ and 4+) of titanium ions. As a result, the chemical solubility limit of $KTaO_3$ gives a maximum value of $n_{3D} = 1.4 \times 10^{20}$ cm^{-3} (ref. 23). However, there is scope for electrostatic doping reaching values of n_{3D} that cannot be achieved with chemical doping.

EDL transistor devices were fabricated on $KTaO_3$ (001) single crystals with an ionic liquid as the electrolyte with a planar device configuration (Fig. 1; see Methods). Excellent transistor characteristics were obtained at room temperature (shown in Supplementary Fig. S1). We observed an abrupt increase in drain current for values of V_G above 2.7 V (and upto 5 V), yielding an on/off ratio as high as 1×10^5. When V_G was too high, a large leakage Faradaic current flowed between the channel and the gate electrode owing to an electrochemical reaction in the ionic liquid. A leakage current larger than 1 μA was observed for V_G above 8 V (Supplementary Fig. S2). Therefore, V_G was limited to below 6 V for all of the experiments shown in this Letter.

Figure 2b,c shows the temperature dependence of transport properties. The channel maintained a metallic state down to 2 K for V_G larger than 2.75 V, whereas the channel was insulating at $V_G = 2.5$ V. We observed a sharp increase in mobility towards low temperatures, as observed in chemically doped crystals[10]. The two-dimensional carrier density n_{2D} was temperature-independent above 140 K and monotonically increased with V_G. However, a peculiar decrease in n_{2D} was observed with decreasing temperature for $V_G > 3.5$ V, saturating below 10 K. Similar temperature dependence was reproducibly observed for all samples. Such

[1]WPI Advanced Institute for Materials Research, Tohoku University, Sendai 980-8577, Japan, [2]PRESTO, Japan Science and Technology Agency, Tokyo 102-0075, Japan, [3]Institute for Materials Research, Tohoku University, Sendai 980-8577, Japan, [4]Center for Low Temperature Science, Tohoku University, Sendai 980-8577, Japan, [5]Quantum-Phase Electronics Center and Department of Applied Physics, The University of Tokyo, Tokyo 113-8656, Japan, [6]Department of Physics, Tohoku University, Sendai 980-8578, Japan, [7]CREST, Japan Science and Technology Agency, Tokyo 102-0075, Japan.
*e-mail: kawasaki@ap.t.u-tokyo.ac.jp

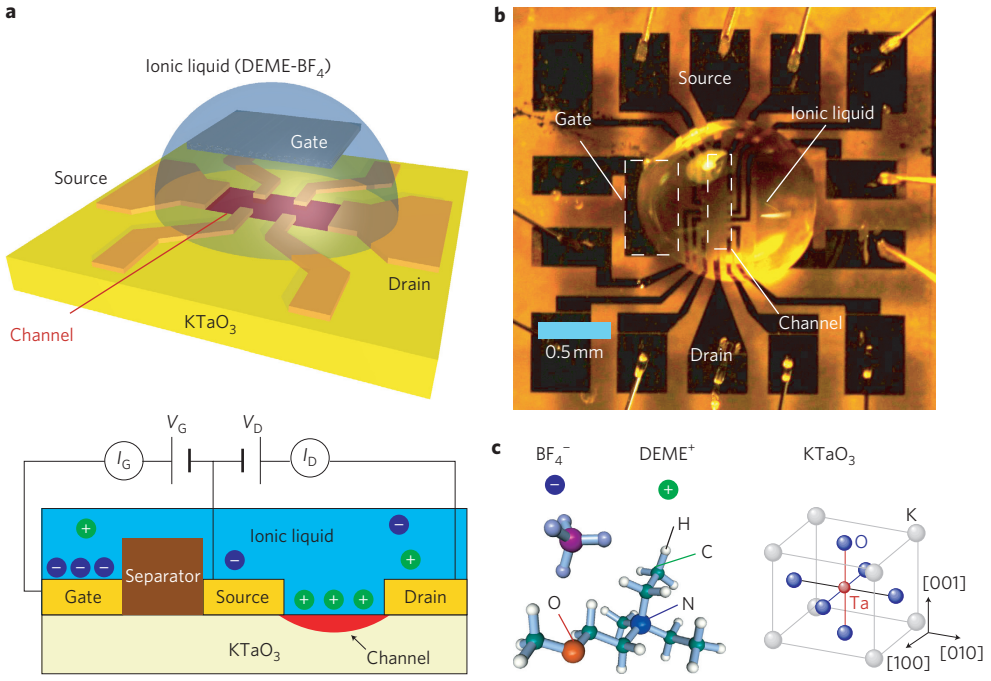

Figure 1 | Electric double-layer (EDL) transistor. a,**b**, Schematic diagrams (**a**) and photograph (**b**) of the EDL transistor with an ionic liquid electrolyte, DEME-BF_4. $DEME^+$ ions comprise the cations and BF_4^- ions ore the anions. The device was fabricated on a $KTaO_3$ single crystal. Source, drain and gate electrodes were fabricated on the crystal (black area in the photograph), and the entire surface of the crystal, except for the channel area and electrodes, was covered by separator layer (yellow area in the photograph). A small amount of the ionic liquid was dropped on the crystal so that it covered the channel region ($KTaO_3$ surface) and the gate electrode. **c**, Molecular and crystal structures for the anion, cation and $KTaO_3$.

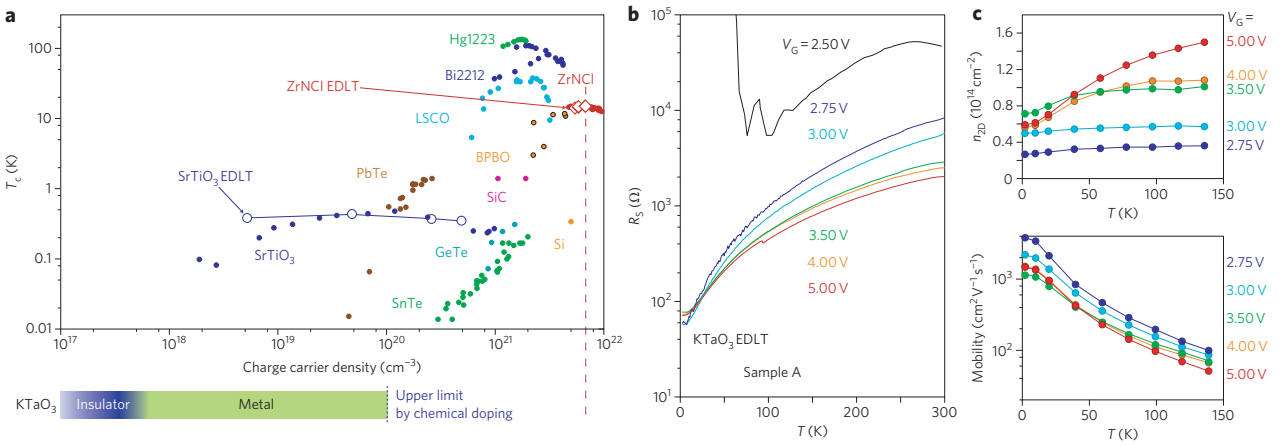

Figure 2 | Characterization of EDL transistors. a, Superconducting critical temperature T_c as a function of three-dimensional charge carrier density for chemically doped superconductivity in 11 different material systems (filled symbols), and electrostatically induced superconductivity in two of these (open symbols). The lower panel shows the electronic phases appearing in $KTaO_3$ as a function of carrier density up to the maximum density that can be achieved with chemical doping: much higher densities are possible with EDL transistors (dashed red vertical line). **b**, Sheet resistance R_S (on a logarithmic scale) versus temperature T at six different gate voltages V_G for an EDL transistor in which the channel is a single crystal of $KTaO_3$. The channel shows metallic conduction for values of V_G higher than a threshold of 2.75 V. **c**, Two-dimensional charge carrier density n_{2D} (top) and carrier mobility (bottom) versus T for five values of V_G: both n_{2D} and mobility were evaluated by Hall measurements.

behaviour was previously reported for two-dimensional conductive layers in $SrTiO_3$, such as niobium-doped thin films[5], delta-doped heterostructures[8], $LaAlO_3/SrTiO_3$ heterostructures[7] and electric-field-induced accumulation layers[6]. Takahashi *et al.* compared the change in the Hall coefficient at various temperatures and electrostatic charging, and concluded that the Hall coefficient above 100 K yields a correct estimate of the carrier density[5]. This phenomenon may be related to the quantum paraelectricity and ferroelectricity induced upon the electric field in these systems. In the following part of this Letter, we use n_{2D} at 100 K as a representative value for the discussion of transport and superconducting properties unless otherwise specified.

The two-dimensional carrier density showed a nearly proportional increase with V_G above a threshold voltage (Fig. 3a). The mobility was as high as 7,000 $cm^2\,V^{-1}\,s^{-1}$ at a low n_{2D} of $2.4 \times 10^{13}\,cm^{-2}$ (Fig. 3b), which is the highest value recorded in two-dimensional systems formed of transition metal oxides. Mobility decreases as a function of n_{2D}. To compare this behaviour with the case of bulk chemical doping, we need to estimate three-dimensional carrier density n_{3D}. For this purpose, we

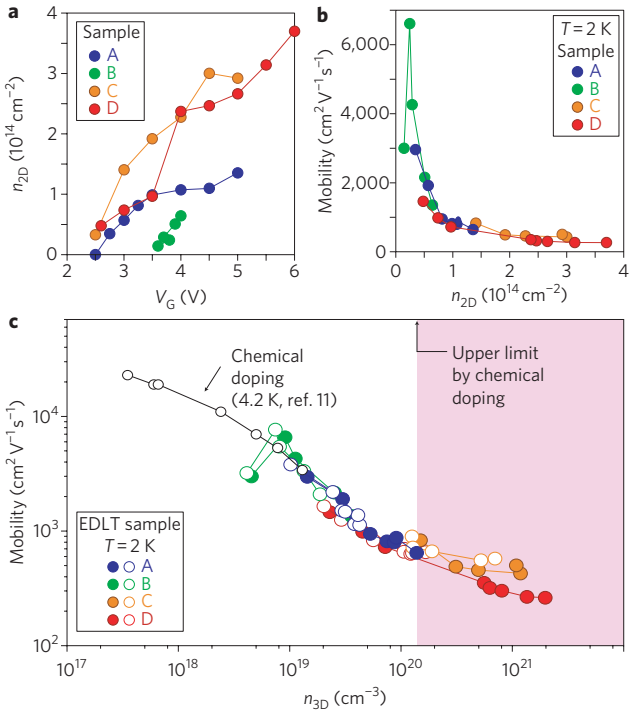

Figure 3 | Transport properties. a, Two-dimensional charge carrier density n_{2D}, deduced from the Hall coefficient at 100 K, versus gate voltage V_G for four different EDL transistors in which the channel is a layer of $KTaO_3$. **b**, Mobility at 2 K versus n_{2D} for the same four samples. **c**, Mobility versus three-dimensional carrier density n_{3D}, deduced from the estimated depth distribution of carriers (see Supplementary Information) for the same four samples: note that both axes are logarithmic. Solid and open symbols correspond to the data deduced from the three-dimensional carrier density n_{3D} determined by the Hall coefficient measured at 100 K and 2 K, respectively. Data for chemically doped bulk $KTaO_3$ crystals from ref. 10 are also shown. Chemical doping in $KTaO_3$ cannot access values of n_{3D} in the shaded area.

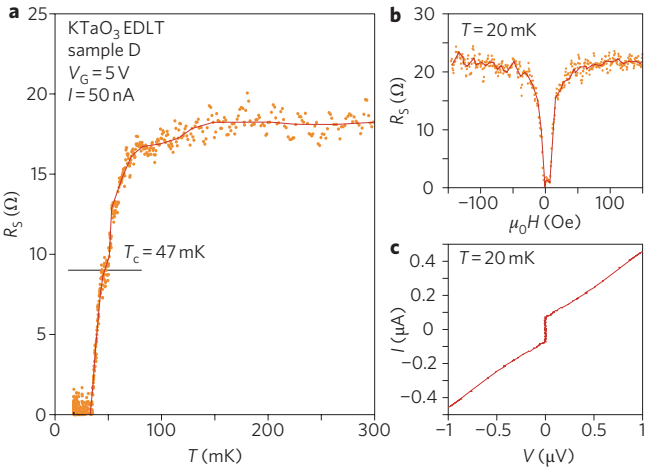

Figure 4 | Superconducting properties. a, Sheet resistance R_S versus temperature T at gate voltage $V_G = 5$ V in an EDL transistor in which the channel is a layer of $KTaO_3$. The solid line denotes the mid-point of the superconducting transition. **b**, R_S versus magnetic field $\mu_0 H$ at 20 mK. **c**, Current I versus differential voltage V at 20 mK, measured in a four-terminal geometry.

performed a sub-band calculation by using reported values of dielectric constant and effective mass. (More details are given in the Supplementary Information and ref. 7.) Figure 3c shows n_{3D} dependence of the mobility for EDL transistors and chemical doping[11]. For EDL transistors, the mobility versus n_{2D} relation agrees well for measurements taken at 100 K (solid symbols, Fig. 3c) and 2 K (open symbols, Fig. 3c). Mobility commonly decreases with increasing n_{3D}, but in convex and concave manners for the chemical doping and EDL transistors, respectively, possibly reflecting the difference in the carrier scattering mechanism: impurity scattering and surface scattering are thought to be dominant in the chemically doped crystals and the EDL transistor, respectively. Here, it should be stressed that n_{3D} obtained by the EDL transistor exceeds the chemical doping limit by an order of magnitude[23]. Although the quantitative accuracy of n_{3D} estimated by means of the sub-band calculation should be re-examined in the future by experimental studies, Fig. 3c strongly indicates that electrostatic doping by the EDL transistor has an ability to go beyond the limit of conventional chemical doping.

Now we show the results measured in a dilution refrigerator for device D with $V_G = 5$ V. Figure 4a shows the temperature dependence of four-terminal sheet resistance R_S, indicating a superconducting transition with an onset at 70 mK and zero resistance at 35 mK. The mid-point critical temperature T_c^{mid} was 47 mK, where $R_S(T_c^{mid}) = 0.5R_S$ (0.2 K). The zero-resistance state was suppressed by application of a small magnetic field above 5 Oe normal to the surface, and R_S returned to the normal state value above 30 Oe, as shown in Fig. 4b. The four-terminal I–V curve in zero field exhibited a supercurrent up to 0.1 μA. These results demonstrate the first observation of superconductivity in $KTaO_3$.

Superconducting properties as a function of carrier density were examined by modulating V_G. Figure 5a shows the temperature dependence of R_S for various values of V_G. No resistance drop was observed for V_G of 3.5 V and 4 V, where n_{3D} was lower than 6×10^{20} cm^{-3}. We therefore conclude that superconductivity in $KTaO_3$ only appears with carrier densities that cannot be achieved by chemical doping[11]. Absence of changes in crystal structure or randomness as a result of chemical doping may be another important factor. In contrast, superconductivity with zero resistance was observed for V_G above 4.5 V. The critical temperature was enhanced at gate voltages from 4 V to 5 V, and then reduced at 6 V. The variation in T_c as a function of V_G is evidence that the superconductivity is not related to other materials produced by a side chemical reaction, such as reduction into tantalum metal ($T_c = 4.4$ K). Figure 5b presents a phase diagram and superconducting critical parameters for $KTaO_3$. The bell-shaped dependence of T_c is similar to that of bulk $SrTiO_3$ crystals, except for the shifts to higher n_{3D} and lower T_c. Both the critical magnetic field $\mu_0 H_c$ and critical current density J_c also show a bell-shaped dependence. The bell-shaped phase diagram is also observed in low-carrier-density superconductors, such as cuprate- and $BaBiO_3$-based superconductors (as shown in Fig. 2a), owing to the emergence of a superconducting state between an electron correlated insulating state and metallic state. It is worth exploring possible common mechanisms behind the bell-shaped phase diagram in $SrTiO_3$ and $KTaO_3$.

We speculate that the difference in their band structures is responsible for the higher n_{3D} required for superconductivity in $KTaO_3$ than that in $SrTiO_3$. Effective masses in $KTaO_3$ are much smaller than those of $SrTiO_3$ (refs 7,24). Smaller effective mass decreases the density of states at the Fermi energy, and thus could decrease the superconducting coupling energy and the critical temperature. In addition, the spin–orbit parameter ξ_{5d} in $KTaO_3$ is one order of magnitude larger than ξ_{3d} in $SrTiO_3$ owing to the heavy tantalum atom, which splits the degenerated conduction band and also decreases the density of states[20]. A detailed band calculation will provide a clear explanation of the difference between $SrTiO_3$ and $KTaO_3$.

In conclusion, the demonstration of superconductivity in $KTaO_3$ clearly shows the potential of electrostatic doping to achieve higher charge carrier densities than is possible with

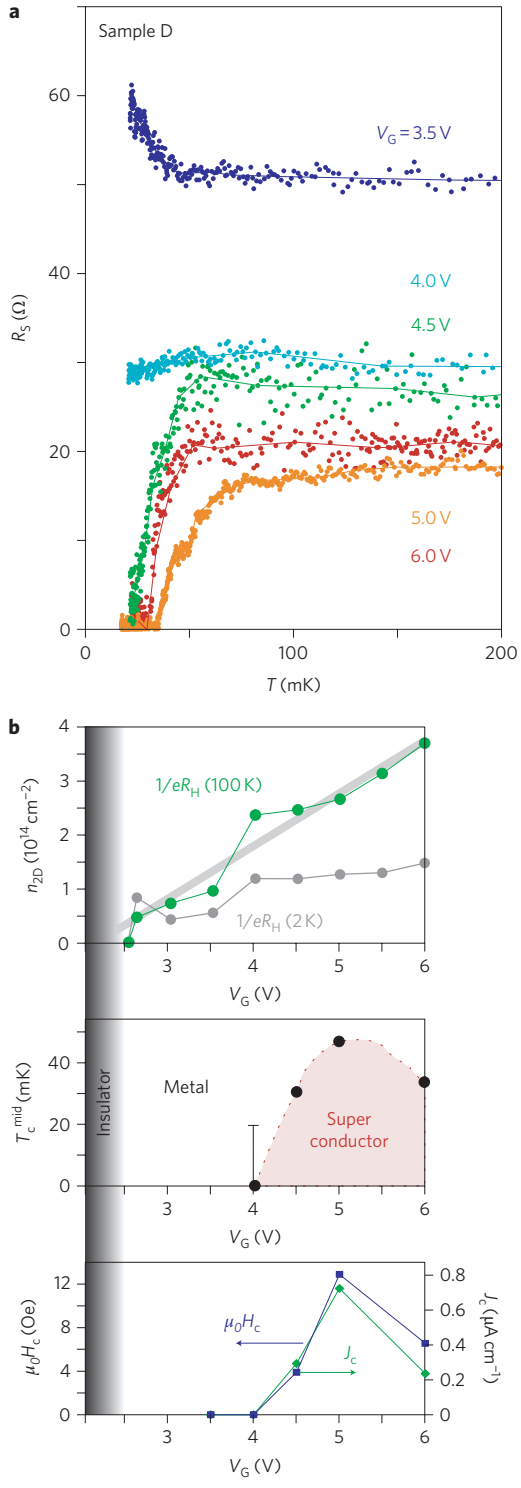

Figure 5 | Transport properties and critical parameters of superconductivity. a, Sheet resistance R_S versus temperature T at five values of the gate voltage V_G. **b**, Two-dimensional carrier density n_{2D} (top panel), mid-point critical temperature T_c^{mid} (middle panel), critical magnetic field $\mu_0 H_c$ (bottom panel, blue; left axis) and critical current density J_c (bottom panel, green; right axis) as a function of gate voltage V_G. Green and grey points in the top panel correspond to data deduced from the Hall coefficient R_H at 100 K and 2 K, respectively. The $KTaO_3$ channel remained insulating at $V_G = 2.5$ V, and n_{2D} was close to zero because of the low temperature. The bar for $V_G = 4$ V in the middle panel indicates uncertainty owing to the minimum accessible temperature of 20 mK. Each critical parameter was deduced from the mid-point of the transition.

chemical doping, which could lead to the discovery of more superconducting compounds.

Methods

Devices were fabricated on $KTaO_3$ (001) single crystals, which had atomically flat surfaces as delivered from the vendor (Furuuch Chemical Co. Ltd). We used a planar device configuration as shown in Fig. 1. In the previous study, we used a platinum wire as a gate and all the components, including substrate, gold wirings to the substrate and the platinum wire, were immersed in an electrolyte[7]. As a result, large leakage current was observed owing to electrochemical reactions between the platinum wire and the gold wirings. In the planar configuration, the gate electrode was fabricated on the substrate and placed near the channel (Fig. 1a). A drop of an ionic liquid (electrolyte) covered only the area between the channel and the gate electrode, and did not contact other electrodes or wirings (Fig. 1b). The leakage current was therefore greatly reduced in comparison with the previous configuration with a platinum wire. Ohmic contact electrodes with a Hall bar geometry were fabricated by electron-beam evaporation of a gold/titanium film, which enabled measurement of the four-terminal resistance and Hall coefficient of the channel. Hard baked photoresist was used for the separator layer between the single crystal and the electrolyte. We selected a sputtered platinum film and an ionic liquid *N*,*N*-diethyl-*N*-(2-methoxyethyl)-*N*-methylammonium tetrafluoro-boron (DEME-BF_4) as the gate electrode and the electrolyte, respectively, owing to their electrochemical stability[25,26].

Received 16 February 2011; accepted 15 April 2011; published online 22 May 2011

References

1. Glover, R. E. & Sherrill, M. D. Changes in superconducting critical temperature produced by electrostatic charging. *Phys. Rev. Lett.* **5,** 248–250 (1960).
2. Mannhart, J., Bednorz, J. G., Müller, K. A. & Schlom, D. G. Electric field effect on superconducting. $YBa_2Cu_3O_{7-\delta}$ films. *Z. Phys. B* **83,** 307–311 (1991).
3. Ahn, C. H. *et al.* Electrostatic modulation of superconductivity in ultrathin $GdBa_2Cu_3O_{7-x}$ films. *Science* **284,** 1152–1155 (1999).
4. Parendo, K. A., *et al.* Electrostatic tuning of the superconductor–insulator transition in two dimensions. *Phys. Rev. Lett.* **94,** 197004 (2005).
5. Takahashi, K. S. *et al.* Local switching of two-dimensional superconductivity using the ferroelectric field effect. *Nature* **441,** 195–198 (2006).
6. Reyren, N. *et al.* Superconducting interfaces between insulating oxides. *Science* **317,** 1196–1199 (2008).
7. Ueno, K. *et al.* Electric-field-induced superconductivity in an insulator. *Nature Mater.* **7,** 855–858 (2008).
8. Kozuka, Y. *et al.* Two-dimensional normal-state quantum oscillations in a superconducting heterostructure. *Nature* **462,** 487–490 (2009).
9. Ye, J. T. *et al.* Liquid-gated interface superconductivity on an atomically flat film. *Nature Mater.* **9,** 125–128 (2010).
10. Wemple, S. H. Some transport properties of oxygen-deficient single-crystal potassium tantalite ($KTaO_3$). *Phys. Rev.* **137,** A1575–A1582 (1965).
11. Thompson, J. R., Boatner, L. A. & Thomson, J. O. Very low-temperature search for superconductivity in semiconducting $KTaO_3$. *J. Low Temp. Phys.* **47,** 467–475 (1982).
12. Yuan, H. T. *et al.* High-density carrier accumulation in ZnO field-effect transistors gated by electric double layers of ionic liquids. *Adv. Func. Mater.* **19,** 1046–1053 (2009).
13. Bednorz, J. G. & Müller. K. A. Possible high T_c superconductivity in the Ba–La–Cu–O system. *Z. Phys. B* **64,** 189–193 (1986).
14. Bhattacharya, A., Eblen-Zayas, M., Staley, N. E., Huber, W. H. & Goldman, A. M. Micromachined $SrTiO_3$ single crystals as dielectrics for electrostatic doping on thin films. *Appl. Phys. Lett.* **85,** 997–999 (1994).
15. Parendo, K. A. *et al.* Electrostatic tuning of the superconductor–insulator transition in two dimensions. *Phys. Rev. Lett.* **94,** 197004 (2005).
16. Caviglia, A. D. *et al.* Electric field control of the $LaAlO_3/SrTiO_3$ interface ground state. *Nature* **456,** 624–627 (2008).
17. Panzer, M. J., Newman, C. R. & Frisbie, D. C. Low-voltage operation of a pentacene field-effect transistor with a polymer electrolyte gate dielectric. *Appl. Phys. Lett.* **86,** 103503 (2005).
18. Shimotani, H., Asanuma, H., Takeya, J. & Iwasa, Y. Electrolyte-gated charge accumulation in organic single crystals. *Appl. Phys. Lett.* **89,** 203501 (2006).
19. Misra, R., McCarthy, M. & Hebard, A. F. Electric field gating with ionic liquids, *Appl. Phys. Lett.* **90,** 052905 (2007).
20. Mattheiss, L. F. Energy bands for $KNiF_3$, $SrTiO_3$, $KMoO_3$, and $KTaO_3$. *Phys. Rev. B* **6,** 4718–4740 (1972).
21. Ueno, K. *et al.* Field-effect transistor based on $KTaO_3$ perovskite. *Appl. Phys. Lett.* **84,** 3726–3728 (2004).
22. Nakamura, H. & Kimura, T. Electric field tuning of spin–orbit coupling in $KTaO_3$ field-effect transistors. *Phys. Rev. B* **80,** 121308 (2009).
23. Sakai, A., Kanno, T., Yotsuhashi, S., Adachi, H. & Tokura, Y. Thermoelectric properties of electron-doped $KTaO_3$. *Jpn J. Appl. Phys.* **48,** 097002 (2009).

24. Uwe, H., Kinoshita, J., Yoshihiro, K., Yamanouchi, C. & Sakudo, T. Evidence for light and heavy conduction electrons at the zone center in $KTaO_3$. *Phys. Rev. B* **19,** 3041–3044 (1979).
25. Kötz, R. & Carlen, M. Principles and applications of electrochemical capacitors. *Electrochim. Acta* **45,** 2483–2498 (2000).
26. Sato, T., Masuda, G. & Takagi, K. Electrochemical properties of novel ionic liquids for electric double layer capacitor applications. *Electrochim. Acta* **49,** 3603–3611 (2004).

Acknowledgements

This work was partly supported by Grants-in-Aid for Scientific Research (21686002, 21224009 and 21654046) and an Innovative Area grant on 'Topological Quantum Phenomena' from the Ministry of Education, Culture, Sport, Science and Technology of Japan. This work was also partly supported by Asahi Glass Foundation and the Nippon Sheet Glass Foundation for Materials Science and Engineering.

Author contributions

K.U. performed planning, sample fabrication, measurements and analysis. S.N., N.K., T.N. and H.A. assisted with cryogenic transport measurements. H.S. and H.T.Y. assisted with planning. Y.I. and M.K. performed planning and analysis.

Additional information

The authors declare no competing financial interests. Supplementary information accompanies this paper at www.nature.com/naturenanotechnology. Reprints and permission information is available online at http://www.nature.com/reprints/. Correspondence and requests for materials should be addressed to M.K.